JOURNAL OF GEOPHYSICAL RESEARCH, VOL. 103, NO. C11, PAGES 25,101–25,108, OCTOBER 15, 1998

Estimation of wind stress using dual-frequency TOPEX data

Tanos Elfouhaily[1]
University Space Research Association, NASA, Greenbelt, Maryland

Douglas Vandemark
NASA Goddard Space Flight Center, Wallops Island, Virginia

Jérôme Gourrion and Bertrand Chapron
Institut Français de Recherche pour l'Exploitation de la Mer, Brest, France

Abstract. The TOPEX/POSEIDON satellite carries the first dual-frequency radar altimeter. Monofrequency (Ku-band) algorithms are presently used to retrieve surface wind speed from the altimeter's radar cross-section measurement (σ^0_{Ku}). These algorithms work reasonably well, but it is also known that altimeter wind estimates can be contaminated by residual effects, such as sea state, embedded in the σ^0_{Ku} measurement. Investigating the potential benefit of using two frequencies for wind retrieval, it is shown that a simple evaluation of TOPEX data yields previously unavailable information, particularly for high and low wind speeds. As the wind speed increases, the dual-frequency data provides a measurement more directly linked to the short-scale surface roughness, which in turn is associated with the local surface wind stress. Using a global TOPEX σ^0 data set and TOPEX's significant wave height (H_s) estimate as a surrogate for the sea state's degree of development, it is also shown that differences between the two TOPEX σ^0 measurements strongly evidence nonlocal sea state signature. A composite scattering theory is used to show how the dual-frequency data can provide an improved friction velocity model, especially for winds above 7 m/s. A wind speed conversion is included using a sea state dependent drag coefficient fed with TOPEX H_s data. Two colocated TOPEX-buoy data sets (from the National Data Buoy Center (NDBC) and the Structure des Echanges Mer-Atmosphere, Proprietes des Heterogeneites Oceaniques: Recherche Experimentale (SEMAPHORE) campaign) are employed to test the new wind speed algorithm. A measurable improvement in wind speed estimation is obtained when compared to the monofrequency *Witter and Chelton* [1991] model.

1. Introduction

The National Aeronautics and Space Administration (NASA) altimeter aboard the TOPEX/POSEIDON satellite is the first operational dual-frequency altimeter. In addition to the nominal Ku-band (2.1 cm) transmit frequency, the altimeter interleaves a C-band (5.5 cm) signal. The primary purpose of the second radar is to provide a colocated ranging measurement to correct for ionospheric path delay in the Ku-band range estimate. This dual-frequency approach has worked well and will be integrated into the next TOPEX-class altimeter, Jason.

Other uses for this TOPEX C-band measurement are being investigated. Rain attenuates the Ku-band return signal much more than at C band. Several studies have shown that the TOPEX radars can be used for rain detection and estimation, as well as storm and global rain climatology studies [*Quartly et al.*, 1996; *Tournadre and Morland*, 1997; *Chen et al.*, 1997]. Use of the dual-frequency ranging data may prove valuable in refining the electromagnetic bias range correction needed to provide accurate Ku-band sea surface height estimates. This paper deals with a third application: use of the two frequencies to refine an altimeter estimate of near-surface wind speed.

It is well-accepted that a monofrequency altimeter's measurement of ocean radar cross section (σ^0) can be mapped directly into an estimate of surface wind speed. At this time the most widely used algorithm is the modified Chelton and Wentz lookup table [*Witter and Chelton*, 1991] (hereinafter referred to as WC91). This empirically derived routine provides an estimate of wind speed at 10 or 19.5 m above the surface. Wind speed estimated by WC91 is generally in agreement with in situ measurements, but there is also evidence to suggest that the altimeter measurement is impacted by additional, non-wind-dependent factors. These factors can include surface current and atmospheric stability [*Vandemark et al.*, 1997], but the largest contaminating factor appears to be the degree of sea state development [e.g., *Glazman and Pilorz*, 1990; *Lefèvre et al.*, 1994], which we will refer to as wave age, normally characterized by the phase speed of the dominant wave divided by the wind speed at a height of 10 m (C_p/U_{10}).

Altimeter ocean backscatter is most simply modeled as the specular backscatter from all surface roughness elements with length scales greater than about 3 times the incident wavelength. Roughness scales of the order of the radar wavelength

[1]Now at Applied Physics Laboratory, Johns Hopkins University, Laurel, Maryland.

Paper number 98JC00193.
0148-0227/98/98JC-00193$09.00

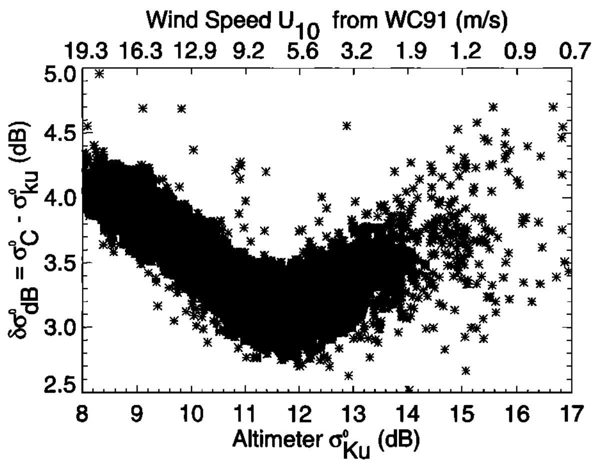

Figure 1. Radar cross-section difference, $\delta\sigma^0_{dB} = \sigma^0_C - \sigma^0_{Ku}$, versus σ^0_{Ku} for TOPEX cycle 70. The top x axis indicates the corresponding wind speed as inferred using the *Witter and Chelton* [1991] (WC91) lookup table and a -0.7 dB bias applied to TOPEX Ku band.

tend to scatter the incident field away from the specular direction and thus reduce the power of the backscatter return. The impact of residual, or nonlocal, sea state on altimeter-estimated wind speed is illustrated by the example where a moderate wind dies quickly to calm. Longer waves (lengths of roughly 20 cm to many meters) would still be present and supporting a roughened surface, while the shortest, most wind-dependent wavelets are absent. In this case an overestimate of wind speed can be expected from the altimeter; the residual sea state is contaminating the local wind information.

Monaldo and Dobson [1989] suggested the use of additional altimeter information, such as the significant wave height (H_s), when estimating the wind speed [e.g., *Lefèvre et al.*, 1994]. *Glazman and Pilorz* [1990] observed that the dimensionless H_s ($\tilde{H}_s = gH_s/U^2_{10}$) could be a pertinent parameter to aid wind speed retrieval. *Ebuchi et al.* [1992] found a significant influence of the fetch on the growth of wind waves and therefore on the wind speed estimation from normalized radar cross-section (NRCS) measurements. A combined study of altimeter and synthetic aperture radar (SAR) over the Golfe du Lion [*Queffeulou et al.*, 1995], along with a theoretical prediction of NRCS function of wind speed and wave age, showed the importance of the degree of development of wind waves. As a result of these studies, it is clear that empirical inversion schemes that involve the wind speed alone can be improved upon, especially near coastal regions. Finally, *Vandemark et al.* [1997] observed that the Ku-band measurements at nadir can be directly related to the wind stress at light to moderate wind speeds.

Bliven et al. [1996] first proposed that a dual-frequency altimeter might be able to correct a monofrequency altimeter wind estimate for residual sea state impacts. Their theoretical study suggested that one could, in addition, extract the surface significant slope from each TOPEX measurement [see, e.g., *Klaassen*, 1994]. Such a result has not yet been realized, but their suggestion that the ratio or difference between the C- and Ku-band signals should carry useful wind-related information is apparent [*Elfouhaily et al.*, 1996]. In this paper we first provide observations and discussion for a global sampling of TOPEX backscatter data at both C and Ku bands along with H_s. The data suggest a means to better isolate the wind-related information contained in the σ^0 measurements. In the section 3, these observations and a theoretical altimeter backscatter model are used to define a dual-frequency wind stress algorithm. Validation of the model against buoy wind measurements is then provided along with closing comments.

2. Exploration of a Dual-Frequency Data Set

A key motivation for this study is the global dual-frequency (C-band (5.5 cm) and Ku-band (2.1 cm)) altimeter data set available from the NASA altimeter (hereafter referred to as TOPEX) aboard the TOPEX/POSEIDON satellite. A dual-frequency altimeter makes six independent measures at a time, three at each frequency. Sea surface height (SSH) is derived from the time delay between transmit and receipt of the echo. Significant wave height (H_s) is deduced from the slope of the leading edge of the returned wave form. The normalized radar cross section (σ^0) is obtained from a mean value of the returned signal power.

For this study, several complete cycles of TOPEX data were extracted from the merged geophysical data records (MGDR) contained on the CD-ROMs distributed by Archivage, Validation et Interprétation des donnêes des Satellites Océanographiques (AVISO). A cycle provides global coverage over a 10-day period. The MGDR data provide estimates at a 1-s rate corresponding to TOPEX σ^0 spatial coverage of ~12 km^2 for a given data point. A nominal TOPEX data cycle contains ~400,000 points on open ocean. The σ^0 data in this paper are slightly modified from MGDR values to provide an improved power calibration as described in the appendix.

It was shown in a previous analysis [*Chapron et al.*, 1995] that TOPEX σ^0_{Ku} and σ^0_C are well correlated; both decrease with increasing wind speed. Such a result was expected because the frequencies are quite close. The interesting observation comes from the change between σ^0_{Ku} and σ^0_C with changing winds. For illustration, Figure 1 shows a scatterplot of

$$\delta\sigma^0_{dB} = (\sigma^0_C)_{dB} - (\sigma^0_{Ku})_{dB} = (\sigma^0_C/\sigma^0_{Ku})_{dB}$$

versus $(\sigma^0_{Ku})_{dB}$ for TOPEX cycle 70, a complete global sampling. The top x axis labels indicate the corresponding surface wind speed that would be estimated from the WC91 σ^0_{Ku} algorithm with a 0.7dB shift [*Callahan et al.*, 1994]. Note that the total range of $\delta\sigma^0_{dB}$ spread is about 1.5 dB and that there is a significant scatter in this quantity for a given σ^0_{Ku}. Figure 1 also indicates that the rate of σ^0 decrease with wind speed differs between the two frequencies depending on the wind speed. Two distinct regimes are identified, occurring about the minimum $\delta\sigma^0_{dB}$ at a wind speed of roughly 7 m/s ($\sigma^0_{Ku} \approx 11.7$ dB). This plot represents the fundamental signature of the dual-frequency TOPEX σ^0, readily repeatable with any particular cycle.

A direct inference from Figure 1 is that the combination of C and Ku bands provides access information related to shorter-scale surface waves of the order of the incident radiation. If such waves were not present, returns at both frequencies would be identical. *Chapron et al.* [1995] applied a theoretical surface scattering model to discuss some of the information contained in Figure 1. In particular, it was pointed out that the critical surface wave length scales of interest for the case of dual-frequency TOPEX analysis lie in the short gravity-capillary wave range. In section 3 this will be discussed in the context of scattering theory.

The TOPEX data set permits a powerful illustration of nonlocal wind impacts by supplying a coincident H_s estimate. As mentioned in the introduction, numerous authors have pointed out an apparent nonwind signature in σ^0_{Ku}-derived wind speed estimates that is attributed to residual sea state influence. Those studies had to rely on altimeter H_s, monofrequency altimeter wind speed, and some form of independent wind speed estimate. Typically, this might be a surface wind model or selected buoy comparisons. Here we utilize TOPEX's $\delta\sigma^0_{dB}$ as the independent wind-related parameter. The results for cycle 70 are shown in Figure 2 and provide a strong indication that σ^0_{Ku} is indeed sea state dependent.

Figure 2a was created from the global data set by binning the data into subsets of ± 0.5 m in H_s and ± 0.5 dB in σ^0_{Ku}. Figures 2b and 2c are expanded and inverted views of Figure 2a to show the low and high wind regimes more clearly. It is apparent that the wind-related parameter $\delta\sigma^0_{dB}$ is multivalued for a given σ^0_{Ku} depending on the value of H_s. The reason for some of the scatter seen in Figure 1 now becomes clear.

In Figures 2a–2c we note that for any value of σ^0_{Ku}, $\delta\sigma^0_{dB}$ is lowered as H_s increases. More specifically, the following observations can be made.

1. Here 12.7 dB $\lesssim \sigma^0_{Ku}$; $\delta\sigma^0_{dB}$ decreases with decreasing σ^0_{Ku} and increasing H_s (see Figure 2b). This branch corresponds to light (or calm) wind conditions ($U_{10} \lesssim 3.75$ m/s) and will not be addressed in this paper. Information on this topic can be found in work by *Vandemark et al.* [1997] and *Gourrion et al.* [1998].

2. Here 11.6 dB $\lesssim \sigma^0_{Ku} \lesssim$ 12.7 dB; a $\delta\sigma^0_{dB}$ plateau is present with little sensitivity to both σ^0_{Ku} or H_s (see Figure 2a). This indicates that in this low wind region (3.75 m/s $\lesssim U_{10}$ 7 m/s) dual-frequency data is insensitive to sea state variations, and therefore traditional algorithms might hold.

3. Here $\sigma^0_{Ku} \lesssim$ 11.6 dB; $\delta\sigma^0_{dB}$ increases with decreasing σ^0_{Ku} and decreasing H_s (see Figure 2c). Most of our attention in section 3 will be focused on this high wind branch ($U_{10} > 7$ m/s);

In this presentation the huge global sampling permits H_s to appear as a surrogate wave age or fetch parameter, where curves of higher H_s roughly represent older seas and curves of lower H_s represent the younger ones. Thus a qualitative interpretation of Figures 2a–2c is that for fixed σ^0_{Ku} the short wave or local wind signature increases (increasing $\delta\sigma^0_{dB}$) with decreasing sea state (decreasing H_s).

Foremost, this global illustration provides strong evidence supporting the influence of longer surface waves on the σ^0_{Ku} measurement. However, it is important to point out that Figure 2 alone does not provide a simple procedure to correct the σ^0_{Ku}-derived wind speed. Each point in these curves is derived from a large statistical sampling having significant scatter (of the order of 0.25 dB root-mean-square (rms)). There is no simple or unique mapping between the three parameters (σ^0_{Ku}, σ^0_C, H_s) and the surface wind speed. This is partially because H_s is known to be an ambiguous wave field descriptor, carrying a mixture of nonlocal swell and wind sea information. One is also without a known relationship between the "wind-related" $\delta\sigma^0_{dB}$ and a geophysical wind estimate. Additionally, this $\delta\sigma^0_{dB}$ signal is quite small with dynamic range of <1.5 dB.

In the following sections we examine these problems with the understanding that Figure 2 suggests a potential in the dual-frequency signals to refine TOPEX wind estimations. Once again, differences between C and Ku bands will be central to the discussion.

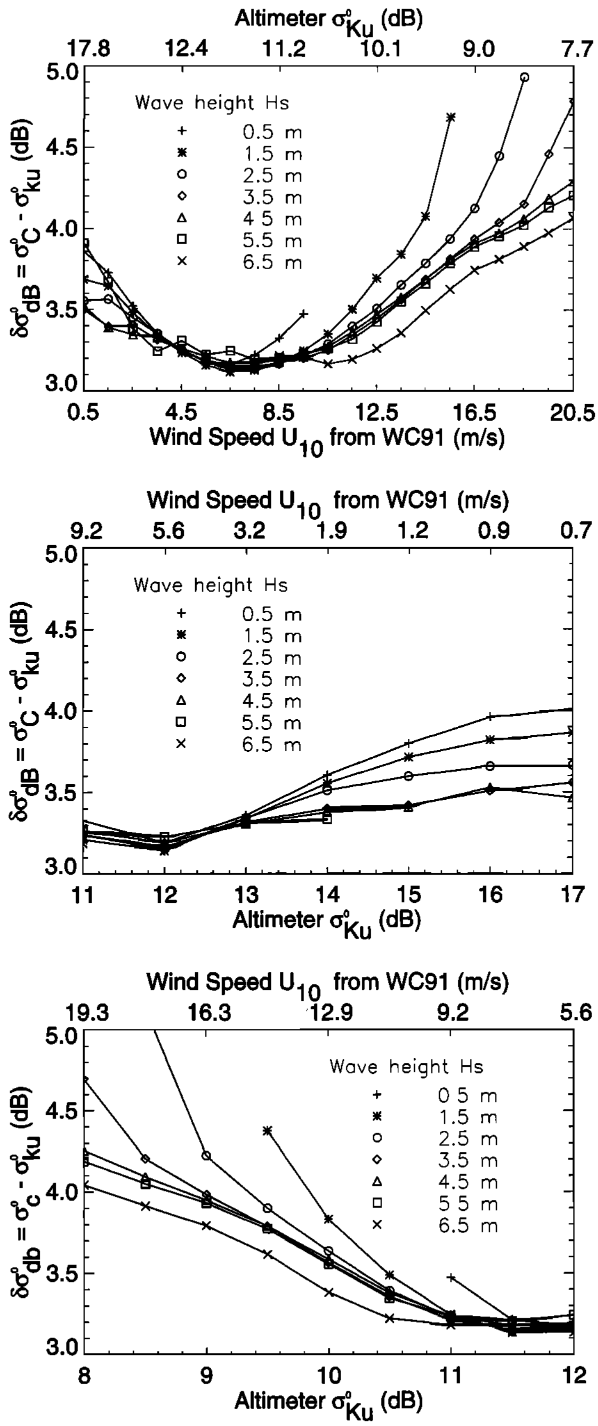

Figure 2. Same as Figure 1 except now $\delta\sigma^0_{dB}$ data are binned (σ^0_{Ku}) and in significant wave height (H_s). The bin size is unity in both σ^0_{Ku} and H_s. (a) Here $\delta\sigma^0_{dB}$ as a function of U_{10} from WC91 for different wave heights. (b) Different scale emphasizing high σ^0_{Ku} (low winds) and (c) different scale emphasizing low σ^0_{Ku} (high winds).

3. A Wind Stress Algorithm for Dual-Frequency Altimeters

A transfer function between surface wind and the couplet (σ^0_{Ku}, σ^0_C) is required to make quantitative use of TOPEX observations. In section 3.1 a scattering model will provide the basis for that function, and sections 3.2 and 3.3 will describe the implementation of a wind stress algorithm.

3.1. Composite Scattering Theory

From the composite surface scattering model [e.g., *Chapron et al.*, 1995] the nadir-looking ocean backscatter cross section is comprised of quasi-specular and diffractive components and can be written as

$$\sigma^0_{\mathrm{em}}(0°) = \frac{|R_{\mathrm{em}}(0)|^2}{\mathrm{mss}_{\mathrm{L-em}}} \exp\left(-4k^2_{\mathrm{em}}\rho_{\mathrm{S-em}}\right) \tag{1}$$

where $\mathrm{mss}_{\mathrm{L-em}}$ is associated with the filtered surface slope variance (mean square slope), $\rho_{\mathrm{S-em}}$ is related to the wave height variance of the smaller scale, k_{em} is the incident electromagnetic wavenumber, and $R_{\mathrm{em}}(0)$ is the corresponding Fresnel reflectivity coefficient at zero incidence angle.

To implement (1) requires defining the long-scale (subscript L) and short-scale (subscript S) regimes. This cutoff wavelength separating long and short scales is well approximated as 3 times the incident wavelength [*Brown*, 1990]. Therefore, for the C- and Ku-band radars, quasi-specular scattering is derived from waves of lengths >16 and 6 cm, respectively. We then deduce that $\mathrm{mss}_{\mathrm{L-C}}$ will be smaller than $\mathrm{mss}_{\mathrm{L-Ku}}$, such that $\mathrm{mss}_{\mathrm{L-Ku}} = (1 + \varepsilon_s)\mathrm{mss}_{\mathrm{L-C}}$. A full evaluation of the cross-section difference using (1) and assuming small ε_s gives

$$\delta\sigma^0_{\mathrm{dB}} = (\sigma^0_{\mathrm{C}}/\sigma^0_{\mathrm{Ku}})_{\mathrm{dB}} \simeq 2.1 \text{ dB} + \frac{10}{\ln 10} \cdot (\varepsilon_s + 4k^2_{\mathrm{Ku}}\rho_{\mathrm{S-Ku}} - 4k^2_{\mathrm{C}}\rho_{\mathrm{S-C}}) \tag{2}$$

where the constant 2.1-dB term is related to the ratio of the effective C/Ku Fresnel coefficients. From the cutoff definition, s represents short gravity and gravity-capillary waves. Use was also made of the approximation $\ln(1 + \varepsilon_s) = \varepsilon_s$.

As suggested by *Cox and Munk*'s [1956] optical measurements over a slick surface, it can be hypothesized that $\mathrm{mss}_{\mathrm{L-C}}$ is only slowly increasing for moderate to high wind speed. In such a case, (2) shows that $\delta\sigma^0_{\mathrm{dB}}$ is dominated by the small-scale slope and height variance covering the range of centimetric waves (about 2–16 cm). These small scales determine to a large extent the air-sea transfer processes and are the waves most closely coupled to wind stress at the surface. As proposed by several authors, the equilibrium short gravity wave spectrum has been shown theoretically and experimentally to be friction velocity (u^*) dependent [e.g., *Phillips*, 1985; *Jähne and Riemer*, 1990]; the different variance parameters entering (2) will then be u^* dependent.

Under low-wind conditions the observed insensitivity of $\delta\sigma^0_{\mathrm{dB}}$ suggests that relative contributions of both long (L) and short scales (S) to the effective mean squared slope are of equal importance. For lighter winds the long wave contribution will further dominate; $\delta\sigma^0_{\mathrm{dB}}$ increases because $\mathrm{mss}_{\mathrm{L-C}}$ is generally smaller for light wind, but $\delta\sigma^0_{\mathrm{dB}}$ can also be lowered as the residual sea state increases (higher H_s).

3.2. Wind Stress Transfer Function

Employing a pragmatic approach based on the previous section and TOPEX observations, we define two new σ^0-related parameters [*Elfouhaily*, 1996]. These parameters are called the sum Σ and the difference Δ of the "effective" mean square slopes calculated from the two frequencies. These parameters are defined as follows. Low winds (3.75 m/s $\lesssim U_{10} \lesssim$ 7 m/s) are

$$\Sigma = \left(\frac{R_{\mathrm{Ku}}}{\sigma^0_{\mathrm{Ku}}} + \frac{R_{\mathrm{C}}}{\sigma^0_{\mathrm{C}}}\right) \times 100 = (\mathrm{mss}_{\mathrm{Ku}} + \mathrm{mss}_{\mathrm{C}}) \times 100 \tag{3a}$$

and high winds (7 m/s $\lesssim U_{10}$) are

$$\Delta = \left(\frac{R_{\mathrm{Ku}}}{\sigma^0_{\mathrm{Ku}}} - \frac{R_{\mathrm{C}}}{\sigma^0_{\mathrm{C}}}\right) \times 1000 = (\mathrm{mss}_{\mathrm{Ku}} - \mathrm{mss}_{\mathrm{C}}) \times 1000 \tag{3b}$$

where $R_{\mathrm{Ku}} \approx 0.38$ and $R_{\mathrm{C}} \approx 0.61$ are effective Fresnel coefficients at nadir for Ku and C bands, respectively [e.g., *Jackson et al.*, 1992]. Also note that here σ^0 quantities are in normal units. In this case the term effective mean square slopes implies $\mathrm{mss}_{\mathrm{Ku}}$ and $\mathrm{mss}_{\mathrm{C}}$ are not only due to slope variances but may also contain a nonnegligible fraction added by the diffraction of the electromagnetic waves over ocean ripples.

In the low-wind regime (3.75 m/s $\lesssim U_{10} \lesssim$ 7 m/s), σ^0_{Ku} and σ^0_{C} contain the same information. A single-frequency model or the two frequencies combined in additive manner should then give similar results. Here we use the sum to provide additional sensor averaging assuming that both frequencies are of comparative quality and noise level.

Light winds ($U_{10} \lesssim$ 3.75 m/s) are not be addressed by the present model mostly because short-scale roughness is difficult to model in a wind-driven wave model. In particular, our input sea surface spectrum [*Elfouhaily et al.*, 1997] does not apply to this extreme condition. The case of light wind is addressed in a sequel paper by *Gourrion et al.* [1998] based on the observations displayed in Figure 2.

A two-branch relationship between the Σ and Δ parameters and u^* can be derived from our input surface spectrum [*Elfouhaily et al.*, 1997] and the composite scattering model as follows. Low regime is

$$\Sigma = \Sigma_m + \Sigma_s \ln \frac{u^*}{c_m} \qquad u^* \leq c_m \tag{4a}$$

and high regime is

$$\Delta = \Delta_m + \Delta_s \ln \frac{u^*}{c_m} \qquad u^* \geq c_m \tag{4b}$$

where $c_m \approx 0.23$ m/s is the minimum phase speed (surface tension dependent). These expressions can be numerically evaluated to determine the constants $\Sigma_m \approx \Delta_m \approx 5$, which are the scaled mean square slopes for low and high regimes in percentage and permillage, respectively, and the scale constants $\Sigma_s \approx 2.5$ and $\Delta_s \approx 12$. Moreover, Σ_s is 5 times smaller than Δ_s (relative to Σ_m and Δ_m), which reflects the change of regimes at about 7 m/s as seen in Figures 1 and 2. Essentially, this algorithm consists of a monofrequency algorithm for low-to-moderate wind speeds and a dual-frequency algorithm for moderate-to-high winds. Note that the model is applicable only for wind speeds above 4 m/s.

3.3. Inversion Scheme

The wind friction velocity is directly deduced from Σ and Δ by inverting (4) as follows. Low regime is

$$u^* = c_m \times \exp\left(\frac{\Sigma - \Sigma_m}{\Sigma_s}\right) \qquad \Sigma \leq \Sigma_m \tag{5a}$$

and high regime is

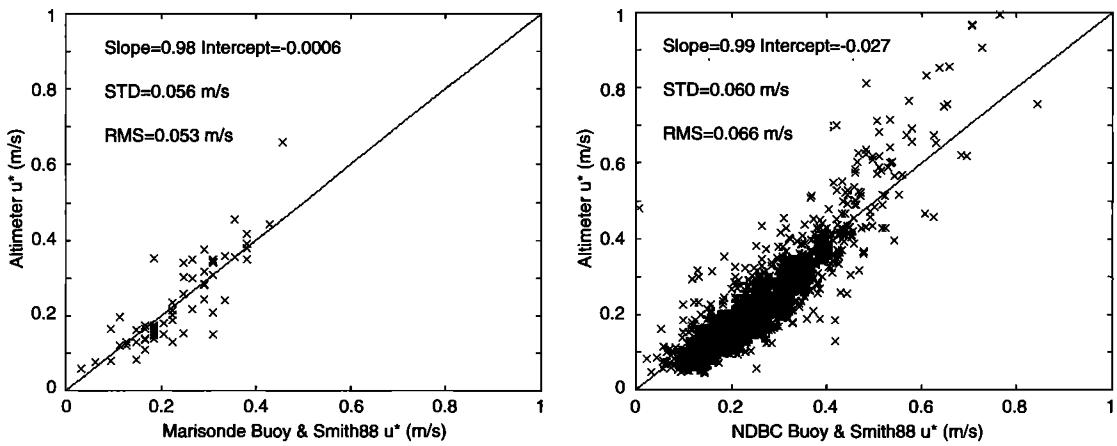

Figure 3. Altimeter wind friction velocity (5) versus buoy friction velocity (u^*) derived from buoy measurements and the *Smith* [1988] drag coefficient. (a) For 65 colocated TOPEX/POSEIDON and Marisonde drifting buoys off the Azores Islands (during the SEMAPHORE campaign, October 1993) and (b) for 1282 colocated points from NOAA NDBC buoys off the U.S. coasts for a duration of 3 years (1993–1995).

$$u^* = c_m \times \exp\left(\frac{\Delta - \Delta_m}{\Delta_s}\right) \qquad \Delta \geq \Delta_m \qquad (5b)$$

These equations indicate that the wind stress for low and high winds increases exponentially with the mean-square-slope sum (Σ in percentage) and difference (Δ in permillage).

In order to test this scheme, in situ u^* measurements are needed for a wide range of ocean conditions. Such a data set is hard to obtain. However one can, as a first approximation, convert the measured buoy U_{10N} to u^* using a traditional drag coefficient. Figure 3 compares altimeter friction velocity (u^*) as inferred from (5) against u^* calculated from buoy wind speed and air-sea temperature measurements assuming the well-known drag coefficient of *Smith* [1988]. Note that this coefficient is sea state independent. The effect of sea state on the drag coefficient will be addressed later in section 4. Two in situ data sets were selected. The first data set is provided by the French Marisonde drifting buoys near the Azores Islands during the Structure des Echanges Mer-Atmosphere, Proprietes des Heterogeneites Oceaniques: Recherche Experimentale (SEMAPHORE) campaign (October–December 1993). This data set mostly contains low-wind conditions. The second data set is a collection of 3 years of measurements (1993–1995) by buoys moored near the U.S. coasts available from the National Data Buoy Center (NDBC). A large diversity of winds and sea states is contained in this data set because of the long period of time (3 years) and because of the various locations (North Atlantic, Gulf of Mexico, North Pacific, and Hawaii).

Overall agreement is obtained between our direct u^* measured by the altimeter and the indirect u^* derived from buoy measurements. The root-mean-square (rms) error is as low as 6 cm/s, which corresponds roughly to 1.6 m/s rms in terms of wind speed U_{10}. This rms is lower than the 2 m/s required for operational algorithms. These results imply that a u^* algorithm from the dual-frequency altimeter of TOPEX is feasible. For this comparison, colocated altimeter data (σ^0_{Ku}, σ^0_C, and H_s) were simply averaged together within 100 km of buoy location and 30 min of buoy measurements. Erroneous altimeter measures are not flagged. The assumption of sea state independent drag coefficient is also a tentative hypothesis that needs a closer examination.

4. Altimeter Local and Neutral Wind Speed

The previous section provided a transfer function to infer wind friction velocity (u^*) from TOPEX measurements by applying (5). A neutral-stability drag coefficient (C_{DN}) is needed in order to estimate the neutral wind speed (U_{10N}). A wind speed estimation can be obtained by using our dual-frequency model (5) in conjunction with a neutral drag coefficient that features the sea state dependence. We suggest in the following a possible approach for defining a drag coefficient that relies on the sea state measured by TOPEX.

Yelland and Taylor [1996] compiled data from two campaigns: the RRS *Discovery* Southern Ocean cruises in the South Atlantic and South Indian Ocean (high sea states), and the French R/V *Le Suroît* in the North Atlantic off the Azores Islands (low winds). They claimed the existence of a robust drag coefficient with no apparent anomaly due to the widely varying sea state conditions. They concluded that for open ocean conditions, where swell is mostly present, a linear drag coefficient to U_{10N} relationship is an excellent fit to their observed data for wind speeds higher than 6 m/s. Below this limit they found a relationship rapidly increasing with decreasing wind speed.

By contrast, *Blake* [1991] reanalyzed three published data sets and detected a wave height (H_s) dependence of the drag coefficient for wind speed higher than 6 m/s. Introducing a wave age parameterization, *Donelan et al.* [1993] also found that wave development affects the wind speed for a given wind friction velocity.

For our suggested model we follow *Smith* [1988] by writing the roughness scale z_0 as the sum of two terms: viscous for laminar flow and Charnock type formulation for rough flow.

$$z_0 = 0.115 \frac{\nu_a}{u^*} + \alpha_c \frac{u^{*2}}{g} \qquad (6)$$

where $\nu_a = 1.4\ 10^{-5}$ m²/s is the air kinematic viscosity. The Charnock parameter α_c is a constant and equals 0.011 in *Smith*'s [1988] formulation. However, according to *Donelan et al.* [1993] and Humidity Exchange Over the Sea (HEXOS) experiment [e.g., *Maat et al.*, 1991], α_c could be a power function of the wave age (C_p/U_{10}). Since the wave age cannot be

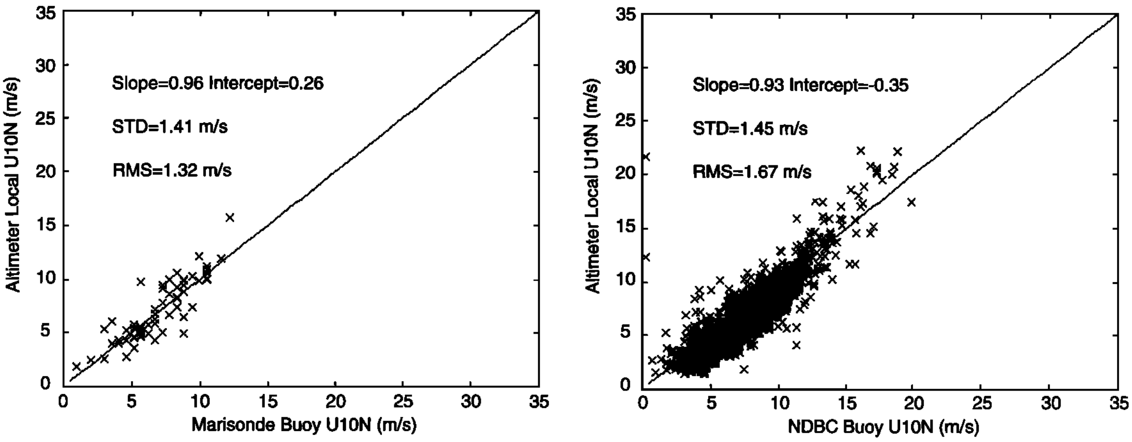

Figure 4. Scatterplot of TOPEX local U_{10N} (5)–(8) (a) versus Marisonde U_{10N} and (b) versus NDBC U_{10N}.

measured by TOPEX, a generalization is made of α_c to be expressed as a power function of the dimensionless significant wave height (see the pseudo wave age definition by *Glazman and Pilorz* [1990])

$$\alpha_c = a(\tilde{H}_s)^{-b} = a\left(\frac{gH_s}{U_{10N}^2}\right)^{-b} \quad (7)$$

with a and b being empirical constants to be determined. Nevertheless, a rough estimation is possible when one considers wind-sea conditions with no swell contamination. In this special case the constants are roughly $a \approx 3 \times 10^{-3}$ and $b \approx 1.0$ ($H_s \approx 0.025U_{10}^2$ for a standard Pierson-Moskowitz situation). The local neutral wind speed is therefore simply derived using the logarithmic wind profile in conjunction with (5), (6), and (7) to be

$$U_{10N} = \frac{u^*}{\kappa} \ln \frac{10}{z_0} \quad (8)$$

where $\kappa \approx 0.4$ is Von Kàrmàn's constant. Since z_0 depends on U_{10N}, u^*, and H_s, an iterative scheme is required to assure convergence toward the local wind speed (U_{10N}) for the local sea state determined by σ^0_{Ku}, σ^0_C, and H_s. A maximum number of iterations, five say, allows detection of inconsistency between the triplet, which may be associated with excessive attenuation due to atmospheric perturbations (e.g., precipitation). From (8) and H_s dependent drag coefficient can be defined, $C_{DN} = [\kappa/\ln(10/z_0)]^2$. This drag coefficient decreases with increasing wave height (H_s) for a given wind speed. It defines an ad hoc drag coefficient for use in wind speed estimation from altimeter measurements.

5. Evaluation

To evaluate our algorithm, we compare a colocation of TOPEX data with two in situ data sets. We use the same SEMAPHORE and NDBC data sets as for section 3.3. Figures 4a and 4b check our model against these in situ measurements. Between buoy and algorithm U_{10N}, rms errors are about 1.32 m/s for Marisonde buoys (Figure 4a) and 1.67 m/s for NDBC buoys (Figure 4b). The *Witter and Chelton* [1991] (WC91) model, based on single-frequency Ku band, gives an rms of 1.94 m/s for the Marisonde buoys and 1.76 m/s for NDBC buoys (Figures 5a and 5b, respectively).

Finally, two cycles (5 and 6) from TOPEX selected over the North Pacific are used to compare the monofrequency and dual-frequency algorithms in Figure 6. Close agreement between our local U_{10N} and the WC91 model is reached for low and moderate winds ($U_{10N} \lesssim 15$ m/s). This confirms our results shown in the previous paragraph when comparing against the buoy measurements. For higher wind speeds, however ($U_{10N} > 15$ m/s), our local U_{10N} significantly diverges from WC91 model. According to *Young* [1993] and *Wu* [1995] models for strong winds our prediction seems to be more realistic

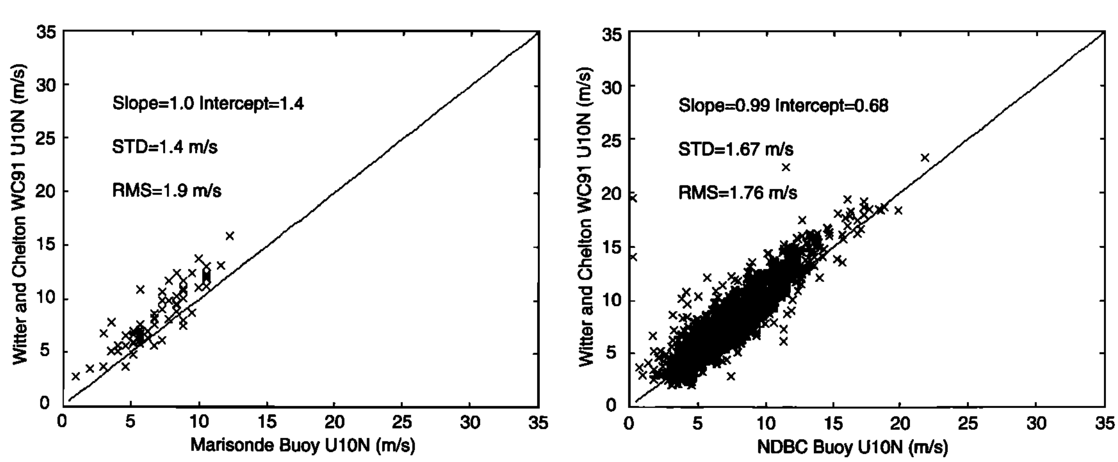

Figure 5. Scatterplot of the WC91 U_{10N} (a) versus Marisonde U_{10N} and (b) versus NDBC U_{10N}.

than those from the operational algorithm (WC91). *Young* [1993] developed a parametric model for winds in hurricane conditions. Figure 6 shows this good agreement. A domain of validity of WC91 could be suggested, according to Figure 6, to be for winds lower than 15 m/s. For higher winds our model provides a smooth transition to Young's hurricane model.

6. Discussion and Conclusion

By utilizing a full cycle of TOPEX MGDR data we have revealed the ability of dual-frequency altimeter measurements to improve local wind speed estimation by reducing the impact of nonlocal sea state signature embedded in a monofrequency altimeter estimates. The parameter $\delta\sigma^0_{dB}(=\sigma^0_C - \sigma^0_{Ku})$ was used to evidence the sea state contamination of wind speed estimates from a monofrequency (Ku-band) algorithm. As the wind speed increases, $\delta\sigma^0_{dB}$ is anticipated to be more directly linked to the short-scale surface roughness and therefore to surface wind stress.

On the basis of this dual-frequency feature, new friction velocity and wind speed algorithms are developed. The friction velocity is directly obtained from the two independent NRCS measurements made by TOPEX: σ^0_{Ku} and σ^0_C. This u^* algorithm is based on the effective mean square slope sum and difference of the dual-frequency NRCS measurements. A fairly low rms error ($\approx$0.06 m/s) is obtained for our u^* estimation when compared to buoy measurements of wind speed by applying a traditional drag coefficient [e.g., *Smith*, 1988]. This algorithm seems to be very robust and gives instantaneous assessment of the wind friction velocity.

Once u^* is estimated from σ^0_{Ku} and σ^0_C, we take advantage of a third independent measurement made by an altimeter: H_s. An iterative scheme is then used to determine a local wind speed U_{10N}, which is sea state dependent. H_s enters into the definition of the roughness scale that induces a drag coefficient that is dependent on sea state through the logarithmic wind profile. The convergence of the local U_{10N} algorithm is very fast, and a few iterations are sufficient. Nonconvergence of this iterative scheme could detect inconsistency between the triplet σ^0_{Ku}, σ^0_C, H_s, which may be associated with excessive attenuations due to atmospheric perturbations (e.g., precipitation). The local U_{10N} is shown to better reproduce in situ measurements than monofrequency algorithms such as, for instance, WC91. An rms of 1.3 m/s is reached under high-sea-state and low-wind situations (e.g., SEMAPHORE campaign) and 1.6 m/s for 3 years of colocated TOPEX-NDBC buoys (see Figures 4 and 5). An implementation of these algorithms in operational routines and even in onboard processing is feasible because of their simplicity and efficiency.

The u^* algorithm for altimeter returns infers wind speeds comparable with buoy and monofrequency algorithms. However, significant divergence from standard inversion models is observed for high winds (>15 m/s). This departure seems to better predict the wind speed under high-wind and sea state situations. The capacity of our model to predict high wind speeds may be a strength of the dual-frequency altimeter. A substantial benefit is therefore provided by our u^* algorithm for future developments of data inversion from microwave instruments.

In conclusion, simultaneous dual-frequency TOPEX data demonstrate the potential to go beyond empirical wind speed relationships. It provides a tool for wind stress estimation based on the difference in sensitivity between the two frequencies. The difference parameter defined in terms of σ^0 values or mean square slopes is directly related to the shortest scales. This parameter is therefore highly sensitive to local perturbations, which act on short waves, while long waves are often the combination of local and nonlocal events.

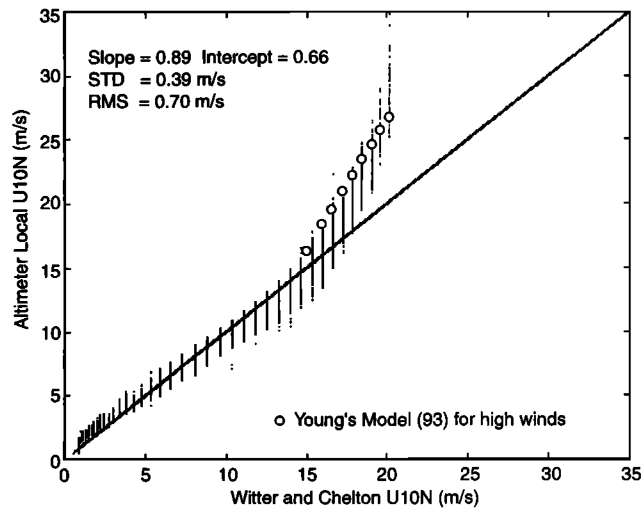

Figure 6. The dual-frequency TOPEX algorithm in terms of local U_{10N} compared to the single-frequency algorithm of WC91 for two cycles (5 and 6) over the North Pacific Ocean. The plot indicates close agreement in the validity domain for WC91 ($\leq$15 m/s) over which our STD was evaluated. The resolution of the plot was imposed by the lookup table of WC91 model, which is of 0.2 dB. While they agree well for moderate winds, our local U_{10N} diverges from WC91 for high winds. The divergence from WC91 appears plausible since it agrees with *Young*'s [1993] model developed for hurricane winds (18 m/s $\lesssim U_{10} \lesssim$ 40 m/s). For higher winds our model presents a smooth transition and a good agreement with Young's model.

Appendix: Recalibration of MGDR σ^0 Values

Values of σ^0 in this paper differ slightly from the MGDR values found on the TOPEX CD-ROMs. For both Ku and C band, all data from a given cycle are put through a refined power calibration lookup table supplied by the TOPEX project (G. Hayne, personal communication, March 1997). This table allows subtraction of the MGDR processing calibration constant and application of a new value on a cycle by cycle basis. The change to MGDR values is usually <0.1 dB.

For the C-band data an additional correction is made. MGDR C-band and Ku-band σ^0 are both corrected for atmospheric (oxygen, moisture, and precipitation) losses using the Ku-band loss term, L^{Ku}_{atm}. This term is derived from the TOPEX microwave radiometer (TMR) data consisting of brightness temperatures at 18, 21, and 37 GHz (T_{18}, T_{21}, T_{37}) and the TMR-derived wet tropospheric range correction, τ_w. The C-band radar is less affected by atmospheric attenuation than the Ku-band system, and the use of L^{Ku}_{atm} introduces error into σ^0_C. A TMR-derived loss term for C band (L^C_{atm}) was supplied in the "GDR users handbook" [*Callahan*, 1993], and our atmospheric C-band correction consists of subtraction of L^{Ku}_{atm} and application of the C-band loss as defined below. The required liquid water (Lz) computation also comes from the

"GDR users handbook." The resulting change to σ_C^0 is about 0.1 dB for clear air, growing to 0.7 dB in strong precipitation.

The positive quantity Lz is defined as follows

$$Lz = -2280.36 - 12.241\,T_{18} - 5.128\,T_{21} + 28.964\,T_{37} \quad \text{(A1)}$$

and

$$L_{\text{bias}} = 0.43\,(Lz - 600) + 0.0003(Lz - 600)^2 \quad \text{(A2)}$$

where if Lz is >600, then Lz becomes $Lz + L_{\text{bias}}$. Finally

$$L_{\text{atm}}^{C} = 8.68589\,(9.87 \times 10^{-3} - 2.17 \times 10^{-2}\,\text{WetTropoRad} + 5.187 \times 10^{-6} Lz) \quad \text{(A3)}$$

Acknowledgments. The authors would like to thank Jean Tournadre and David Cotton for providing the buoy data sets for SEMAPHORE and NDBC, respectively. We are also grateful to colleagues at IFREMER for the helpful comments and valuable discussions. The authors are also indebted to the reviewers for their helpful hints and advice. Contributions of R. Sterner, D. Porter, R. Chapman, E. Dobson, and D. Thompson to improving the layout of the paper are appreciated. This work was supported by IFREMER and NASA Physical Oceanography Program.

References

Blake, R. A., The dependence of wind stress on wave height and wind speed, *J. Geophys. Res.*, *96*, 20,531–20,545, 1991.

Bliven, L. F., P. Sobieski, A. Guissard, and H. Branger, Friction velocity estimation using dual-frequency altimeter data, in *The Air-Sea Interface*, edited by M. A. Donelan, W. H. Hui, and W. J. Plant, pp. 755–760, Univ. of Toronto Press, Toronto, Ont., 1996.

Brown, G. S., Quasi-specular scattering from the air-sea interface, in *Surface Waves and Fluxes*, vol. 2, *Remote Sensing*, edited by G. L. Gernaert and W. J. Plant, pp. 1–39, Kluwer Acad., Norwell, Mass., 1990.

Callahan, P. S., GDR users handbook, *Rep. JPL D-8944*, rev. A, Jet Propul. Lab., Pasadena, Calif., 1993.

Callahan, P. S., C. S. Morris, and S. V. Hsiao, Comparison of TOPEX/POSEIDON σ_0 and significant wave height distributions to Geosat, *J. Geophys. Res.*, *99*, 25,015–15,024, 1994.

Chapron, B., K. Katsaros, T. Elfouhaily, and D. Vandemark, A note on relationships between sea surface roughness and altimeter backscatter, in *Air-Water Gas Transfer: Selected Papers From the Third International Symposium on Air-Water Gas Transfer, Heidelberg University*, edited by B. Jähne and E. C. Monahan, pp. 869–878, AEON Verlag, Hanau, Germany, 1995.

Chen, G., B. Chapron, J. Tournadre, K. Katsaros, and D. Vandemark, Global oceanic precipitation: A joint view by TOPEX and TMR, *J. Geophys. Res.*, *102*, 10,457–10,471, 1997.

Cox, C., and W. Munk, Slopes of the sea surface deduced from photographs of sun glitter, *Bull. Scripps Inst. Oceanogr.*, *6*(9), 401–488, 1956.

Donelan, M. A., F. W. Dobson, S. D. Smith, and R. J. Anderson, On the dependence of sea surface roughness on wave development, *J. Phys. Oceanogr.*, *23*, 2143–2149, 1993.

Ebuchi, N., H. Kawamura, and Y. Toba, Growth of wind waves with fetch observed by Geosat altimeter in the Japan Sea under winter Monsoon, *J. Geophys. Res.*, *97*, 809–819, 1992.

Elfouhaily, T., A consistent wind and wave model and its application to microwave remote sensing of the ocean surface, Ph.D. thesis, 230 pp., Inst. Fr. de Rech. pour l'Exploit. de la Mer, Brest, France, 1996.

Elfouhaily, T., B. Chapron, V. Kerbaol, J. Gourrion, J. Tournadre, K. Katsaros, and V. Vandemark, Dependence of altimeter returns on wind stress and wave age, in *Proceedings of International Geoscience and Remote Sensing Symposium*, vol. II, pp. 1389–1391, IEEE Press, Piscataway, N. J., 1996.

Elfouhaily, T., B. Chapron, K. Katsaros, and D. Vandemark, A unified directional spectrum for long and short wind-driven waves, *J. Geophys. Res.*, *102*, 15,781–15,796, 1997.

Glazman, R. E., and S. H. Pilorz, Effects of sea maturity on satellite altimeter measurements, *J. Geophys. Res.*, *95*, 2857–2870, 1990.

Gourrion J., B. Chapron, T. Elfouhaily, and D. Vandemark, Sea state dependency of dual-frequency altimeter measurements, *Phys. Chem. Earth*, in press, 1998.

Jackson, F. C., W. T. Walton, D. E. Hines, B. A. Walter, and C. Y. Peng, Sea surface mean square slope from K_u-band backscatter data, *J. Geophys. Res.*, *97*, 11,411–11,427, 1992.

Jähne, B., and K. S. Riemer, Two-dimensional wave number spectra of small-scale water surface waves, *J. Geophys. Res.*, *95*, 11,531–11,546, 1990.

Klaassen, E., Windspeed retrieval based on dual-frequency altimetric data: A feasibility study, thesis report, 49 pp., Dep. of Telecommun. and Teledetection, Univ. Cath. de Louvain, Louvain-la-Neuve, Belgium, July 1994.

Lefèvre, J. M., J. Barckicke, and Y. Ménard, A significant wave height dependent function for TOPEX/POSEIDON wind speed retrieval, *J. Geophys. Res.*, *99*, 25,035–25,046, 1994.

Maat, N., C. Kraan, and W. A. Oost, The roughness of wind waves, *Boundary Layer Meteorol.*, *54*, 89–103, 1991.

Monaldo, F., and E. Dobson, On using significant wave height and radar cross section to improve radar altimeter measurements of wind speed, *J. Geophys. Res.*, *94*, 12,699–12,701, 1989.

Phillips, O. M., Spectral and statistical properties of the equilibrium range in the wind-generated gravity waves, *J. Fluid Mech.*, *156*, 505–531, 1985.

Quartly, G. D., T. H. Guymer, and M. A. Srokosz, The effects of rain on TOPEX radar altimeter data, *J. Atmos. Oceanic Technol.*, *13*, 1209–1229, 1996.

Queffeulou, P., T. Elfouhaily, V. Kerbaol, P. Le Borgne, and J. M. Lefèvre, Remote sensing of wind and wave over the Western Mediterranean Sea, paper presented at ESA Proceedings of the 2nd ERS Pilot Project Workshop, Eur. Space Agency, London, Dec. 6–8, 1995.

Smith, S. D., Coefficients for sea surface wind stress, heat flux, and wind profiles as a function of wind speed and temperature, *J. Geophys. Res.*, *93*, 15,467–15,472, 1988.

Tournadre, J., and J. C. Morland, The effect of rain on TOPEX/Poseidon altimeter data: A new rain flag based on Ku and C band backscatter coefficients, *IEEE Trans. Geosci. Remote Sens.*, *35*, 1117–1135, 1997.

Vandemark, D., J. B. Edson, and B. Chapron, Altimeter estimation of sea surface wind stress for light to moderate winds, *J. Atmos. Oceanic Technol.*, *14*, 716–722, 1997.

Witter, D. L., and D. B. Chelton, A GEOSAT altimeter wind speed algorithm and a method for altimeter wind speed algorithm development, *J. Geophys. Res.*, *96*, 8853–8860, 1991.

Wu, J., Microwave specular reflections from breaking waves—Measurements of hurricane winds from space, *J. Phys. Oceanogr.*, *25*, 3231–3236, 1995.

Yelland, M., and P. K. Taylor, Wind stress from the open ocean, *J. Phys. Oceanogr.*, *26*, 541–558, 1996.

Young, I. R., An estimate of the GEOSAT altimeter wind speed algorithm at high wind speeds, *J. Geophys. Res.*, *98*, 20,275–20,285, 1993.

B. Chapron and J. Gourrion, Institut Français de Recherche pour l'Exploitation de la Mer, IFREMER Centre de Brest, Océanography Spatiale, 29280 Plouzané, France. (e-mail: bchapron@ifremer.fr)

T. Elfouhaily, Applied Physics Laboratory, Johns Hopkins University, 11100 Johns Hopkins Road, Laurel, MD 20723-6099. (e-mail: elfoutm1@nansen.jhuapl.edu)

D. Vandemark, NASA Goddard Space Flight Center, Wallops Flight Facility, Wallops Island, VA 23337.

(Received March 21, 1997; revised October 17, 1997; accepted January 16, 1998.)